DOI: 10.1002/cmdc.200500032

Detection of Overexpressed COX-2 in Precancerous Lesions of Hamster Pancreas and Lungs by Molecular Imaging: Implications for Early Diagnosis and Prevention

Hildegard M. Schuller,*[a] George Kabalka,[b] Gary Smith,[b] Arjun Mereddy,[b] Murthy Akula,[b] and Maria Cekanova[a]

The enzyme cyclooxygenase-2 (COX-2) is overexpressed in many cancers, cardiovascular disease, neurodegenerative disorders, and arthritis. Selective inhibitors of COX-2 have been developed as therapeutics or preventive agents for these diseases. However, recent reports have revealed a significant increase in cardiovascular mortality in long-term users of the COX-2 inhibitors Vioxx and Celebrex, emphasizing the need for noninvasive tests that allow the identification of individuals whose COX-2 levels are overexpressed prior to assignment to treatment with these drugs. In this study, we have prepared a radioiodinated analogue of the selective COX-2 inhibitor celecoxib, and verified its binding to the COX-2 enzyme in vitro. Biodistribution studies in hamsters demonstrated significantly higher levels of radiotracer in animals treated with the tobacco carcinogen NNK in lung, pancreas, and liver. Assessment of COX-2 levels by whole-body planar nuclear imaging two hours after injection of the radiotracer was suggestive of a distinct increase in COX-2 in the pancreas and liver of a hamster treated for 10 weeks with NNK, in the lungs and liver of a second animal, and in the liver only, in two additional animals from the same treatment group. Immunostains showed selective overexpression of COX-2 in pre-neoplastic lesions of the pancreas and lungs in only those animals that showed tracer accumulation in these organs and in the livers of all NNK-treated hamsters. Immunostains for COX-1 yielded detectable reactions in the intestinal epithelium but not in pancreas, lungs, or liver, supporting the specificity of the tracer for COX-2. Our data provide proof of principle for the hypothesis that molecular imaging with radiolabeled COX-2 inhibitors can be used for the noninvasive monitoring of overexpressed COX-2 levels.

Introduction

The arachidonic acid-metabolizing-enzyme cyclooxygenase-2 (COX-2) is overexpressed in a significant proportion of cancers, particularly adenocarcinomas of the lungs, breast, stomach, pancreas, colon, and prostate.[1–6] COX-2-mediated metabolism of arachidonic acid (AA) results in the formation of prostaglandins, other prostanoids, and thromboxanes.[7,8] While prostaglandins have been identified as potent growth factors for the family of adenocarcinomas,[9–12] other prostanoids and thromboxanes are important to maintain cardiovascular and renal function.[13–15] Numerous experimental, clinical, and epidemiological studies have provided evidence that inhibitors of COX-2 may decrease the risk for the development of adenocarcinomas.[4,5,10,16,17] However, the potential use of this class of agents for cancer prevention has been challenged by recent reports that the long-term usage of the selective COX-2 inhibitors VIOXX and Celebrex significantly increased cardiovascular mortality.[18,19] This finding emphasizes the need to monitor COX-2 levels in individuals at risk for the development of cancer, prior to assignment to chemopreventive therapy with a COX-2 inhibitor as well as during treatment. Noninvasive molecular imaging with a suitably labeled COX-2 inhibitor would be an ideal tool to achieve this goal if it is sensitive enough to detect increases in COX-2 expression prior to the development of overt cancer.

The nicotine-derived nitrosamine 4-(methylnitrosamino)-1-(3-pyridyl)-1-butanone (NNK) induces adenocarcinomas in the lungs and pancreas of Syrian golden hamsters and other rodent species.[20] Immunohistochemical analyses have shown that these tumors overexpress COX-2.[17,21] In the current study, we have used NNK-treated hamsters to test the hypothesis that elevated COX-2 levels in target organs can be detected by planar nuclear medicine imaging prior to the development of overt cancer, using radioiodinated derivatives of celecoxib **1a** and **1b**.

[a] *Dr. H. M. Schuller, Dr. M. Cekanova*
Department of Pathobiology, College of Veterinary Medicine
University of Tennessee, 2407 River Drive
Knoxville, TN 37996 (USA)
Fax: (+1) 865 974 5616
E-mail: hmsch@utk.edu

[b] *Dr. G. Kabalka, Dr. G. Smith, Dr. A. Mereddy, Dr. M. Akula*
Department of Nuclear Medicine, Graduate School of Medicine
University of Tennessee, Knoxville, TN (USA)

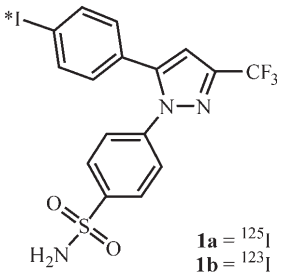

Results

Analysis of the in vitro binding assay showed a time-dependent increase of radioactivity bound to the filters in NNK-treated cells, in agreement with the published ability of this carcinogen to induce COX-2 expression (Figure 1). Pre-incubation

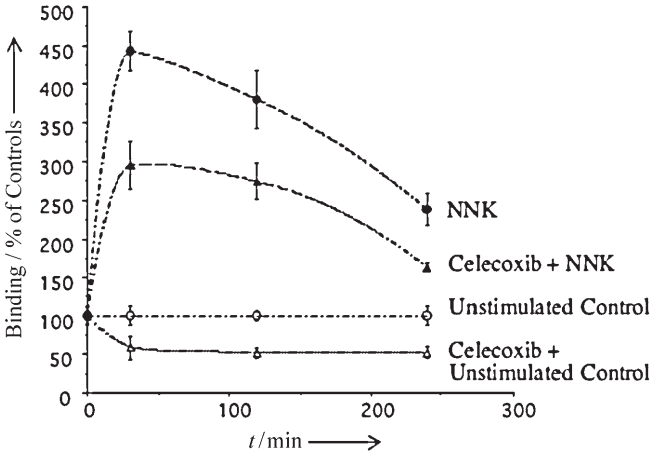

Figure 1. Results of in vitro binding assay. NCI-H322 cells were incubated with [^{125}I]celecoxib in 96-well plates in the presence or absence of the COX-2 inducer NNK (100pM), and cell lysates were harvested onto filters at the time intervals specified. Radioactivity bound to the filters was significantly greater in NNK-treated cells at all time intervals tested, an effect significantly ($p < 0.001$) reduced by pre-incubation of the cells with nonradioactive celecoxib (1 μM). Pre-incubation of non-NNK-treated control cells with nonradioactive celecoxib also significantly ($p < 0.001$) reduced radioactivity bound to the filters. These findings support the interpretation that the radiotracer is bound to the COX-2 enzyme. Data are mean values and standard errors of triplicate samples.

with nonradioactive celecoxib (1 μM) significantly reduced this response ($p < 0.001$) at all time intervals (Figure 1). In addition, base level binding of the radiotracer in unstimulated control cells was significantly ($P < 0.001$) reduced by pre-incubation with nonradioactive celecoxib (Figure 1).

The hamsters used for the biodistribution study weighed from 125 to 130 g. This preliminary study served to confirm that NNK induced the COX-2 enzyme in the expected organs of hamsters used in the current imaging studies. Analysis of the biodistribution of the iodine-125 analogue, **1 a**, in control versus NNK pretreated hamsters demonstrated a time-dependent increase in blood and tissue from lungs, liver, and pancreas of all animals (Figure 2). The blood levels of radioiodinated celecoxib were not statistically different between control and NNK pretreated hamsters except for the last time interval tested (120 min). In contrast, NNK-pretreated hamsters showed a significant ($p < 0.001$) increase of **1 a** at all time intervals with the peak value being a 2.3-fold increase over control values in the lungs at the 120 min time interval. A similar increase was observed at this time interval in the liver (2.9-fold, $p < 0.01$). Pancreatic tissue from NNK pretreated hamsters demonstrated the highest increase (11-fold, $p < 0.001$) over control values 120 min after injection of the radiotracer, with significantly elevated levels relative to controls evident as early as 60 min after tracer administration (Figure 2).

The hamsters used for whole body planar nuclear imaging (Figure 3, 4, and 7) weighed from 125 to 160 grams. Significant levels of tracer were detected in all control hamsters subjected to whole body planar nuclear imaging two hours after subcutaneous injection of iodine-123 labeled **1 b**, but only at the injection site (Figure 3). Immunohistochemistry confirmed the absence of COX-2 overexpression in pancreas (Figure 5 C), liver (Figure 5 D), and lungs (Figure 8 D) of these animals. Of the hamsters euthanized by CO_2, one NNK-treated animal demonstrated accumulated tracer in the liver and pancreas (Figure 4). Immunohistochemical analysis of lungs, liver, and pancreas of this animal confirmed overexpression of COX-2 in liver and pancreas (Figure 5 and 6) and the absence of COX-2 overexpression in the lungs. Quantitative densitometric analysis of liver and pancreas in control and the NNK-treated hamster showed that COX-2 expression was increased 5-fold in multiple focal areas of pancreatic acinar cells of the NNK-treated animal, and a diffuse 2.3-fold increase in all hepatocytes of the liver (Figure 6). Interestingly, the focal areas of COX-2 overexpression in the pancreas were associated with the presence of pseudo-ducts (Figure 5 A), an abnormality often observed at an early stage of experimentally induced pancreatic carcinogenesis. One of the remaining two NNK pretreated hamsters euthanized by CO_2 showed accumulation of tracer in the liver that correlated with diffuse overexpression of COX-2 at this organ site by immunohistochemistry. The third NNK-pretreated hamster did not overexpress COX-2 in any organ by immunohistochemistry, and did not show accumulation of the tracer by whole-body planar nuclear medicine imaging at sites other than that of the subcutaneous injection. Contrary to the data generated in the biodistribution study, none of the NNK-treated animals euthanized by CO_2 showed tracer accumulation in the lungs. Immunohistochemical analysis of these lung tissues failed to detect COX-2 but did show extensive damage to lung tissue, including emphysema and interstitial edema, suggestive of CO_2-related pulmonary hyperacidosis that may have destroyed the COX-2 enzyme, resulting in a false negative reaction to the tracer and the antibody. In support of this interpretation, both NNK-treated hamsters euthanized by an anesthetic overdose showed tracer accumulation in the liver (Figure 7), and one of these animals additionally demonstrated tracer accumulation in the right lung (Figure 7). Immunohistochemical stains revealed one cox-2 positive adenoma (0.5 cm diameter) in the accessory lobe of the right lung (Figure 7 A and 8 A), and eight cox-2 positive micro-adenomas (0.1–0.2 cm in diameter) scattered throughout the remaining lobes of the right lung

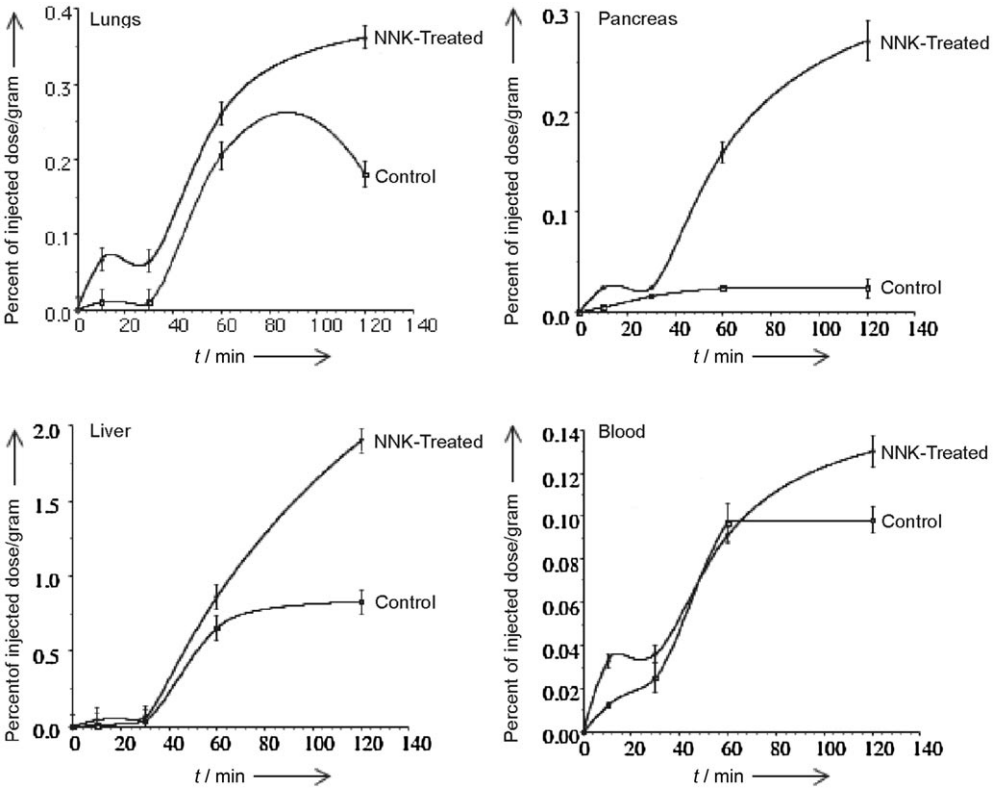

Figure 2. Results of biodistribution study. Control hamsters (15) and hamsters (15) treated for two weeks with NNK (2.5 mg/per100 g bodyweight three times a week) were injected with [^{125}I]celecoxib (3.7 MBq) and sacrificed at the time intervals indicated (three hamsters per time interval for the control and NNK group). Radioactivity in target organs known to respond with an induction of COX-2 to NNK (lung, liver, pancreas) was significantly higher after 60 and 120 min. Data are expressed as mean values and standard errors in percent of the injected dose per gram organ weight.

lary pattern with single layers of epithelial tumor cells surrounded by abundant connective tissue stroma (Figure 8A and B). Lung tissue from the control hamster showed no detectable immunoreactivity to COX-2 antibody in the lung parenchyma while the airway epithelia demonstrated weak positive immunoreactivity (Figure 8D). Both NNK-treated hamsters showed positive immunoreactivity in all hepatocytes, (Figure 8C) whereas no positive reaction was detected in the liver of the control hamster. Densitometric analysis of the immunostains after background subtraction, revealed that the increase in COX-2 expression in the liver of NNK-treated hamsters was 2.9-fold, and 4.4-fold in the epithelial tumor cells of the lung adenomas (Figure 9). Immunostains with a primary antibody to COX-1 demonstrated pronounced base level expression in the intestinal epithelial lining in all control or NNK-treated animals (see Figure 10a). In contrast, COX-1 was below detectable levels in the pancreas, lungs, and liver of control and

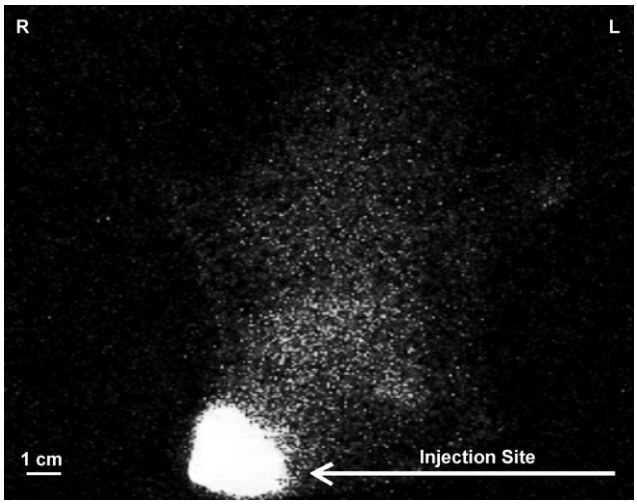

Figure 3. Whole-body planar nuclear image of a control hamster (bodyweight: 125 g) euthanized by CO_2 inhalation two hours after subcutaneous injection of [^{123}I]celecoxib. Note accumulated radioactivity only at the subcutaneous injection site in the right inguinal region (arrowed).

(Figure 7B and 8B) in the hamster that had shown tracer accumulation in the lungs (Figure 7). As is typical for NNK-induced lung tumors in this species, the tumors demonstrated a papil-

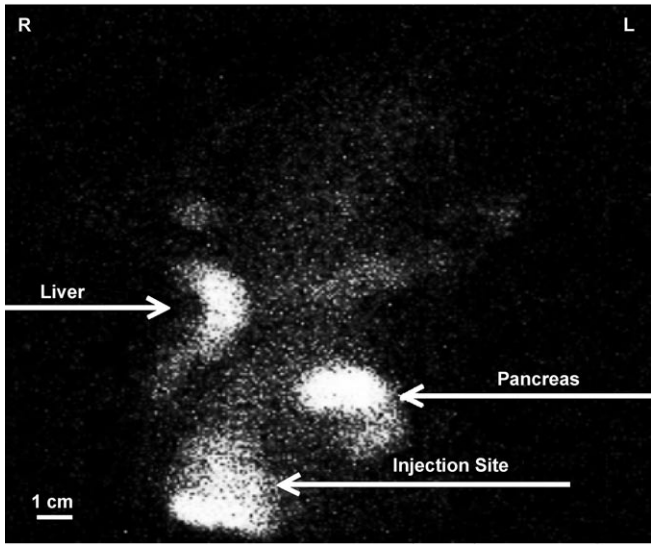

Figure 4. Whole-body planar nuclear image of a hamster (bodyweight; 140 g) pre-treated for 10 weeks with NNK (2.5 mg/100 g bodyweight three times a week) and euthanized by CO_2 inhalation two hours after subcutaneous injection of [^{123}I]celecoxib. Note accumulated radioactivity in liver and pancreas in addition to the subcutaneous injection site.

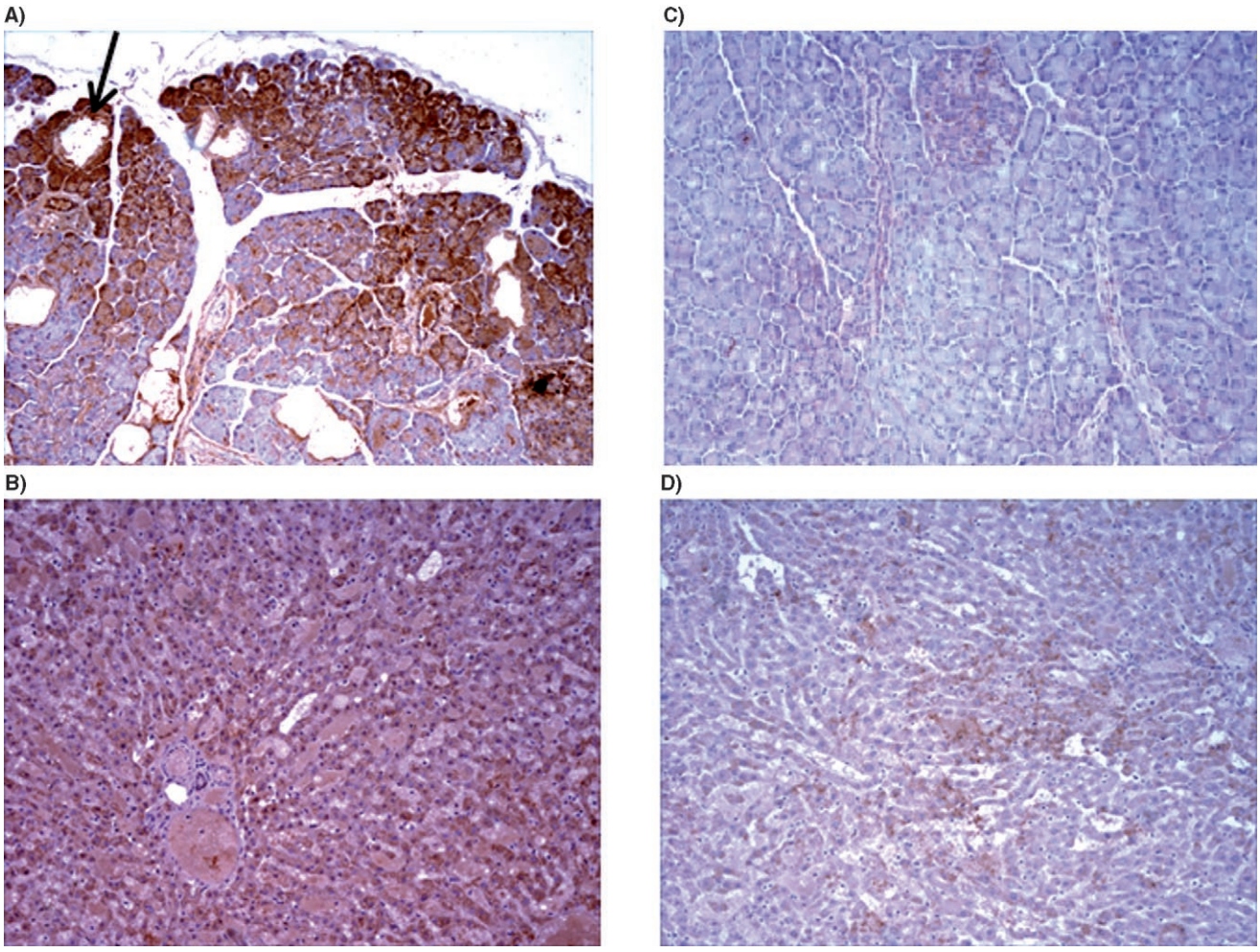

Figure 5. Photomicrographs illustrating immunostains with an anti-COX-2 antibody. A) Pancreatic tissue from the NNK-pretreated hamster shown in Figure 4 demonstrates multiple foci of acinar cells overexpressing COX-2 (brown stain) and formation of pseudo-ducts (exemplified by arrow). B) The liver tissue from the same animal demonstrates diffuse overexpression of COX-2 compared with C) pancreatic and D) liver tissue from a control hamster shown in Figure 3.

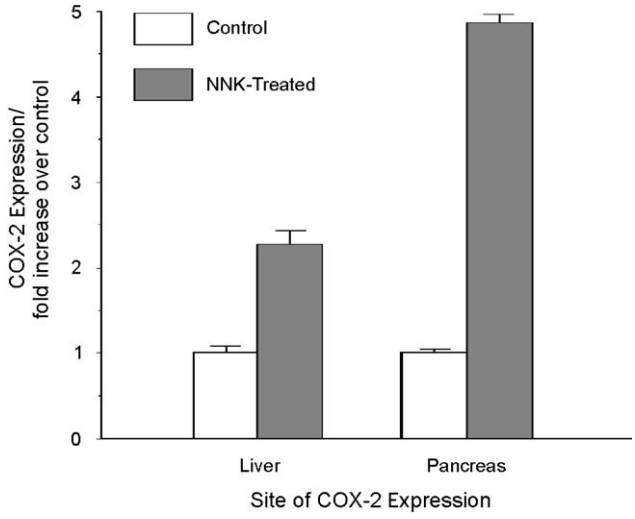

Figure 6. Results of densitometric evaluation of immunostains illustrated in Figure 5, using the NIH Scion Image Analysis software. The COX-2 positive foci in the pancreas demonstrated a five-fold increase relative to identical tissue type in control hamsters, whereas overexpression in the hepatocytes of the liver was 2.3-fold. Bars are mean values and standard errors of 25 densitometric area measurements of standard size.

NNK-treated hamsters (see Figure 10b). This finding corroborates the specificity of tracer binding to the COX-2 enzyme as no tracer accumulation was observed in the intestines of any hamster.

Discussion

Our data show that overexpression of COX-2 can be detected by molecular imaging technology in pre-malignant lesions, prior to the presence of overt cancer in the pancreas and lungs. Other laboratories have reported the synthesis and validation of labeled COX-2 inhibitors as radiotracers for nuclear medicine imaging, including PET. Some of these publications only reported the synthesis of these agents without biological validation.[22,23] The in vivo evaluation of 18F-desbromo-DuP-697 as a PET tracer for COX-2 expression demonstrated high nonspecific uptake of the tracer in the intestines,[24] which would severely limit its use for the detection of COX-2 positive tumors or pre-malignant lesions in the abdominal region. Studies using the 18F-labelled COX-1 and COX-2 inhibitors SC63217 (COX-1) and SC58125 (COX-2) reported in vitro uptake and

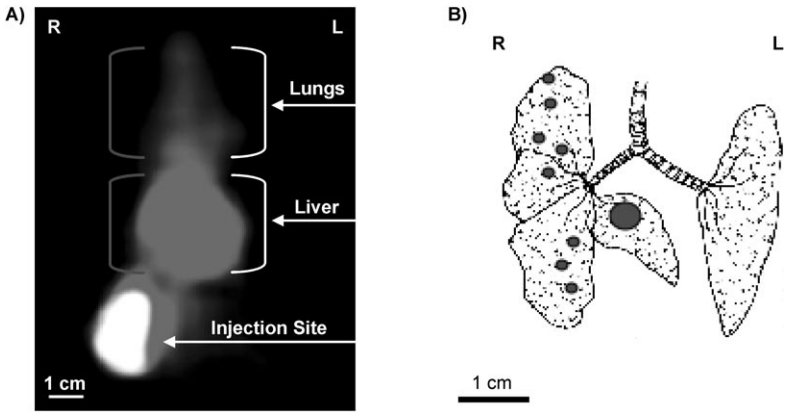

Figure 7. A) Whole-body planar nuclear image of a hamster (bodyweight 160 g) pretreated for 10 weeks with NNK (2.5 mg/100 g bodyweight three times a week) and euthanized by im injection with an anesthetic (telazal) overdose two hours after subcutaneous injection of [^{123}I]celecoxib. Note accumulated radioactivity in the right lung, liver, and at the subcutaneous injection site. B) The schematic drawing illustrates the localization and approximate size of the COX-2 positive pre-malignant lesions (adenomas) in the lungs.

in vivo biodistribution data indicative of selective binding of each tracer to its respective enzyme. However, PET imaging with the COX-2 tracer failed to show tracer accumulation in the brain (an organ with regions of known high COX-2 expression) of a baboon.[25] COX-2 overexpression in animals with fully developed tumors was detected with 99 m Tc-labeled celebrex.[26] In contrast, the current experimental protocol revealed tracer accumulation in pre-malignant lesions of the lungs and pancreas. Notably, the relatively low dose of tracer used (3.7 MBq) allowed for the selective detection of only organ sites with significantly overexpressed COX-2 levels (pre-malignant lesions in lungs and pancreas, elevated COX-2 levels in the liver, and at the subcutaneous injection site), whereas organs with physiologically slightly elevated COX-2 levels (brain, kidneys, airway epithelia) did not show detectable tracer accumulation. Tracer accumulation was stronger in the COX-2 positive liver and pancreatic lesion than in the lung adenomas. This was because of the fact that in ade-

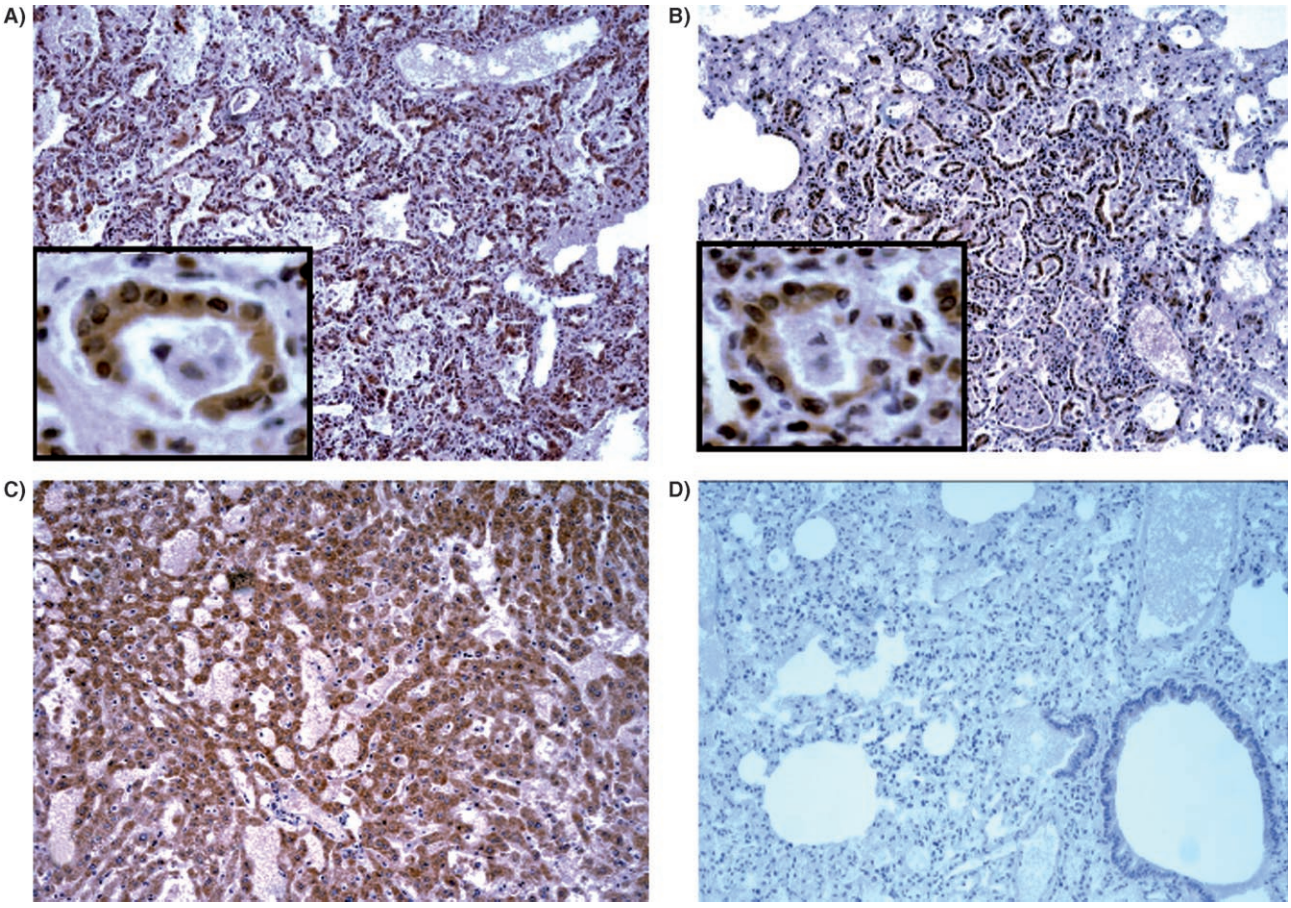

Figure 8. Photomicrographs illustrating immunostains with an anti-COX-2 antibody. Positive immunoreactivity of the lung adenoma (0.5 cm in diameter) located in the accessory lobe of the right lung (Figure 7) is illustrated in A and one of the micro-adenomas (0.2 cm in diameter) in the upper right lobe is illustrated in B. As is typical for NNK-induced lung tumors, the adenomas demonstrated a glandular growth pattern with single central layers of COX-2 positive epithelial tumor cells (insets) surrounded by abundant cox-1 negative stroma. Part C demonstrates positive immunoreactivity of hepatocytes in the liver of the same animal. Part D illustrates weak positive immunoreactivity to COX-2 in the airway epithelia and absence of immunoreactivity in alveolar tissues of a control hamster euthanized by anesthetic overdose.

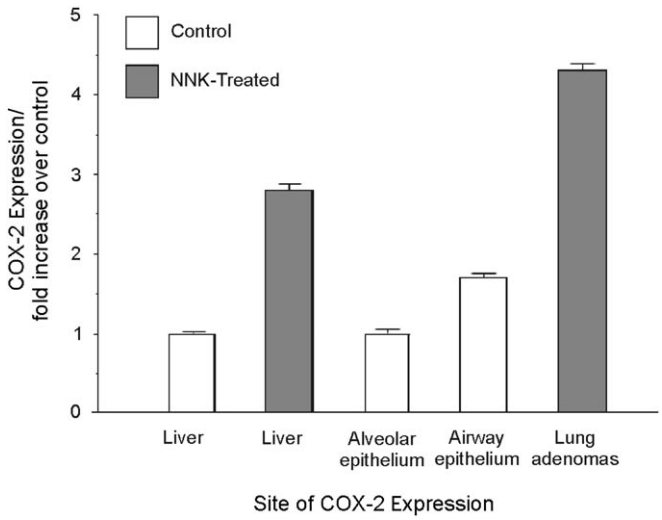

Figure 9. Results of densitometric evaluation of immunostains illustrated in Figure 8, using the NIH Scion Image Analysis software. The COX-2 positive tumor cells in the lung adenomas demonstrated a 4.4-fold increase versus control alveolar tissue and a 2.5-fold increase versus control airway epithelium, while overexpression in the hepatocytes of the liver was 2.9-fold. Bars are mean values and standard errors after background subtraction of 20 densitometric area measurements of standard size.

nomas, only the epithelial tumor cells in very small pre-neoplastic lesions overexpressed COX-2, whereas the abundant tumor stroma and lung parenchyma were COX-negative. In contrast, every single hepatocyte overexpressed the enzyme in the liver of NNK treated hamsters, making this organ a large source of radioactivity. The correlation of tracer accumulation with immunohistochemically detected COX-2 overexpression, in conjunction with the absence of tracer at sites of high COX-1 expression (intestines), provide additional proof for the selective binding of the tracer to the COX-2 enzyme. The significant inhibition of tracer binding observed in the in vitro assays using a human lung adenocarcinoma cell line that overexpresses COX-2, supports this interpretation. Binding of tracer was not completely blocked by pretreatment of the cells with non-radioactive celecoxib, because the highest non-toxic concentration (1 μM) tolerated by these cells did not completely block the enzyme.

Even though whole body planar nuclear imaging is a relatively crude technique when compared with more sophisticated methods such as micro-PET or micro-SPECT, the current data provide evidence that, in principle, organ-specific elevations in COX-2 levels associated with disease can be detected at an early stage by noninvasive imaging technology. This is an important finding in that it provides a tool for the identification of individuals with elevated COX-2 levels at specific organ sites associated with the development of diseases that overexpress the enzyme. Pre-malignant lesions that precede the development of NNK-induced adenocarcinoma of the pancreas and lungs of hamsters only serve as non-limiting examples. Among the diseases that frequently overexpress COX-2, are the most common human cancers such as adenocarcinomas of the lungs, breast, stomach, pancreas, colon, and prostate,[2–5,16] cardiovascular[13,27,28] and neurodegenerative diseases,[29,30] and arthritis.[31,32] However, not all patients with such diseases overexpress COX-2. Treatment with COX-2 inhibitors of individuals not overexpressing the enzyme is not beneficial, and may even be harmful as it decreases COX-2 levels below the physiological levels necessary to maintain cardiovascular and renal function. As the reports of cardiovascular deaths associated with long-term use of the COX-2 inhibitors VIOXX and Celebrex exemplify,[18,19,33] non-selective treatment of patients suffering from diseases associated with increased COX-2 without testing for the actual enzyme levels before and during therapy, can have very serious side effects. On the other hand, there are numerous reports that have documented the benefits of COX-2 inhibitors as therapeutic[30–32,34] and chemopreventive agents.[4,5,10,16] A complete ban of this family of drugs would therefore deprive the medical community, and the patient, of a valuable tool to combat diseases responsive to COX-2 inhibitors. Molecular imaging is an ideal tool for this approach be-

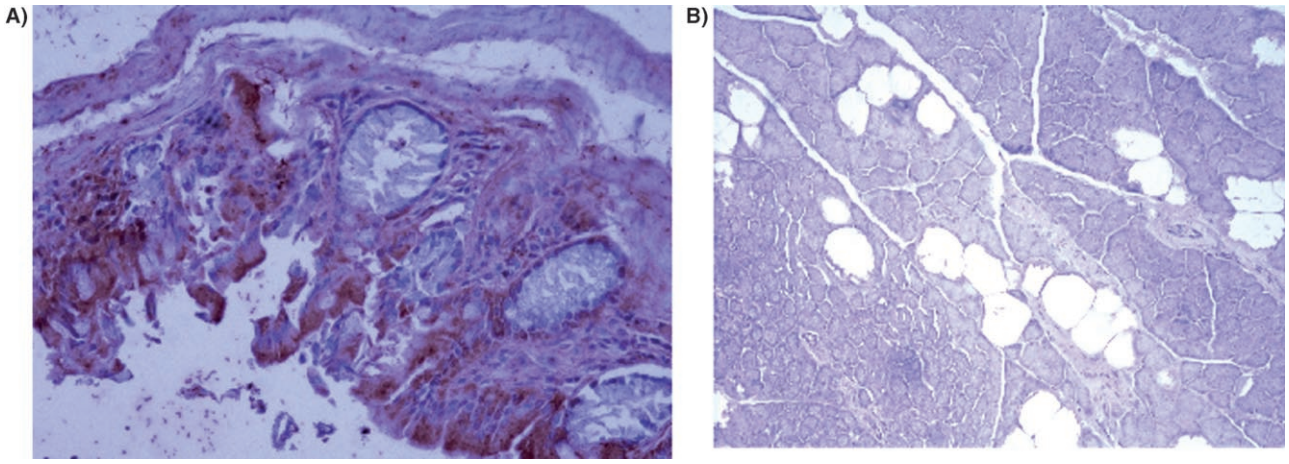

Figure 10. Photomicrographs demonstrating immunostains with an anti-COX-1 antibody. A) The epithelium of the intestines showed pronounced base level expression of the enzyme in all hamsters. B) By contrast, COX-1 was below detectable levels in the pancreas of control and NNK-treated hamsters. As no tracer accumulation was observed in the intestines by whole-body planar nuclear imaging, this finding serves to further corroborate the specificity of tracer for COX-2 (compare with Figure 3, 4, and 7).

cause it is noninvasive, highly specific, allows for the identification of the organ sites involved, the half-life of the isotopes used are short, and the amount of active COX-inhibitor used is much smaller than therapeutic doses.

The current data do not allow for immediate extrapolation to human patients because of the subcutaneous administration route of the tracer. The blood clearance and target/blood ratios of the tracer require additional evaluation after intravenous injection. In addition, labels other than radioiodine may be preferable for the use of celecoxib as an imaging agent in human patients because of the slow blood clearance of this tracer due to its affinity to carbonic anhydrase in erythrocytes.[35]

Experimental Section

Synthesis of radiotracers: Elemental analyses were performed by Atlantic Micro Labs, Inc. Melting points were recorded on an electrothermal Digital Melting Point Apparatus and are uncorrected. ^{1}H and ^{13}C spectra were recorded on a Bruker AC 250 MHz NMR spectrometer. The chemical shift values are expressed in parts per million relative to tetramethylsilane. Radioactivity measurements were made using a Radioisotope Calibrator Model CRC-127R, Capintec Instruments Inc. All starting materials were purchased from Aldrich Chemical Company, $Na^{125}I$ (specific activity $81.4X10^{3}$ GBq mmol^{-1}) was obtained from Amersham Biosciences, $Na^{123}I$ (specific activity $71.4X10^{6}$ GBq g^{-1}) was obtained from Nordion Inc. All reactions were carried out using dry solvents under an inert atmosphere.

*4-[5-(4-[^{125}I]Iodophenyl)-3-trifluoromethyl-pyrazol-1-yl]benzenesulfonamide (**1a**)*: 4-[5-Ttrimethylstannylphenyl)-3-trifluoromethylpyrazol-1-yl]benzenesulfonamide (precursor **5**, 2.8 mg, 5.2 mol, in 100 μL methanol) was prepared according to published procedures [22], placed in a 2 mL Wheaton vial containing no-carrier-added $Na^{125}I$ (9.3 MBq in 0.1% aqueous NaOH). To this, peracetic acid (100 μL, 0.3% solution in methanol) was added. The reaction vial was sealed, covered with aluminum foil, and the mixture stirred for 5 min at room temperature. A drop of 10% aqueous sodium thiosulfate was added to decompose the excess iodine, and the radioiodinated product was isolated by passing it through two silica gel Sep-pak columns using ethyl acetate/hexane (2:1) as eluent. This process removed all ionic materials including residual iodide and separated the product ($R_f = 0.62$) from the tin precursor ($R_f = 0.69$). Three 2 mL fractions were collected. Precursor **5** was found in the first and second fraction, the second fraction contained small quantities of **5** and **1a**. The third fraction contained pure **1a** (as determined by TLC of the fraction and NMR analyses of control reactions carried out with stable sodium iodide). The overall radiochemical yield was determined to be 90% and radiochemical purity of the third fraction was >98%. The total synthesis time was 30 min.

*4-[5-(4-[^{123}I]Iodophenyl)-3-trifluoromethyl-pyrazol-1-yl]benzenesulfonamide (**1b**)*: The synthesis of **1b** was carried out in a parallel fashion as described in an earlier report.[22] The decay corrected radiochemical yield was determined to be 90% and radiochemical purity was >98%. The total synthesis time was 15 min.

In vitro binding study: To verify binding of the radiolabeled celecoxib to COX-2, a human lung cancer cell line (NCI-H322) derived from a pulmonary adenocarcinoma and overexpressing the COX-2 enzyme was used. Cells (30000 cells per well) were seeded into 96-well plates and allowed to attach for 24 h. Cells were then washed twice with PBS, and the radioiodinated analogue **1a** (0.075 MBqi/well) was added in the presence or absence of the tobacco carcinogen (4-methylnitrosamino)-1-(3-pyridyl)-1-butanone (NNK, 100 pM), that induces COX-2. To verify the specificity of binding, untreated cells or cells treated with NNK were pre-incubated for 10 min with nonradioactive celecoxib (1 μM) followed by incubation with the radiotracer for 10 min to 2 h. Cells were then lysed and harvested onto filters with two washes in PBS (Packard Micromate harvester). Radioactivity bound to the filters was measured with a gamma counter.

Biodistribution study: Six-week-old male outbred Syrian golden hamsters were purchased from Charles River (Wilmington, DL). The animals were housed three per cage in plastic shoebox-type cages under standard laboratory conditions and were given unlimited access to food (Purina rodent chow) and tap water. The animals were randomly assigned to two groups, each consisting of 15 hamsters. One group was given NNK (2.5 mg in 0.1 mL saline/100 g bodyweight three time a week for two weeks) by subcutaneous injection. The control group received identical injections of the vehicle (saline). One day after the last NNK injection, the control and NNK-pretreated hamsters were weighed and then given a single subcutaneous injection with 100 μL of a saline solution containing 3.7 MBq of the radioiodinated analogue **1a**. The subcutaneous route (as opposed to intravenous) of drug administration was chosen because hamsters require anesthesia to surgically access the saphenous vein due to the lack of a tail vein. In turn, the anesthesia may alter the biodistribution of the tracer. In small rodents such as rat, mouse, and hamster, the biodistribution of radiolabeled tracer after sc injection is similar to that after intravenous injection.[23] Three hamsters from each of the two groups were sacrificed by isofluorene inhalation while receiving the radiotracer injection (time 0), 30, 60, and120 min after administration of the radioiodinated celecoxib. A blood sample was aspirated from the left ventricle of the heart. The vascular system was then flushed with PBS via the left ventricle under opening of the caudal vena cava to remove circulating blood from liver, lungs, and pancreas. Lungs, liver, and pancreas were harvested and weighed. The radioactivity in each sample was quantified with a gamma counter and expressed as mean values with standard errors of percent of injected dose per gram. Statistical analysis of data was by one way ANOVA and Tukey–Kramer multiple comparison test.

Whole-body planar nuclear imaging: Eight-week-old male outbred Syrian golden hamsters were subcutaneously injected with NNK at a dosage of 2.5 mg in 0.1 mL saline per 100 g bodyweight three times a week for 10 weeks. Age-matched controls were given identical injections with the vehicle (saline). One day after the last injection, the hamsters were weighed and then injected subcutaneously in the right inguinal region with 100 μL of a saline solution containing 3.7 MBq of iodine-123 labeled analogue **1b**. Two hours after injection of the tracer, three NNK treated and three control hamsters were sacrificed by CO_2 asphyxiation. A whole-body planar nuclear medicine image of each hamster was obtained using an Argus Epic gamma camera (Phillips Medical Systems Inc.) equipped with a pinhole collimator. Images were obtained using a 128×128 matrix for 10 min with a photopeak centered at a 159 keV ± 10% energy window. As the nuclear medicine scans and immunohistochemistry indicated potential false negative reactions in the lungs, caused by deterioration of COX-2 resulting from CO_2-induced pulmonary hyperacidosis (see results), two additional NNK-treated and one control hamster were imaged following euthanasia by intramuscular injection of an overdose of anesthetic (telazal) two hours after sc injection of radiotracer.

Immunohistochemistry: After allowing the radioactivity to decay for 10 days in a freezer at −20 °C, the bodies were thawed in a refrigerator at 4 °C overnight. Lung, liver, pancreas, and intestines were then harvested from each hamster, fixed in 10% buffered formalin for 24 h, and processed for microscopic analysis of immunostained paraffin-embedded tissue slides. Deparafinized sections were rinsed in distilled water, then PBS, followed by incubation with 3% H_2O_2 in 50% MeOH at room temperature for 20 min. Incubation with a primary anti-COX-2 rabbit polyclonal antibody (Santa Cruz Biotechnology) that recognizes amino-acids 50–111 of the amino terminus of COX-2 (dilution 1:25, overnight at 4 °C) or with a primary anti-COX-1 rabbit polyclonal antibody that recognizes amino acids 63–124 of COX-1 (Santa Cruz Biotechnology), was followed by two rinses in PBS and incubation for 30 min at room temperature with super sensitive link-biotinylated anti-rabbit immunoglobulin (BioGenex). This was followed by two rinses with PBS and incubation for 30 min at room temperature with super sensitive label-peroxidase-conjugated streptavidin (BioGenex). The slides were then rinsed twice with PBS, incubated with diaminobenzidine solution (Vector) for 7 min at room temperature, rinsed in PBS, then rinsed in distilled water and counterstained with hematoxylin (Richard Allen Scientific). Slides processed in an identical manner but without exposure to the primary antibody served as a negative control. Quantitative densitometric analysis of the immunostains was done using the NIH Scion image analysis software. Statistical evaluation of these data after background subtraction was by one way ANOVA and Tukey-Kramer multiple comparison test.

Acknowledgements

We thank the National Institutes of Health (R01-CA 096128-01A1, RO1-CA 088809, RO1-CA 042829) and the Robert H. Cole Foundation for supporting this research.

Keywords: molecular imaging · precancerous lesions · radioiodinated celecoxib

[1] K. El-Bayoumy, M. Iatropoulos, S. Amin, D. Hoffmann, E. L. Wynder, *Cancer Res.* **1999**, *59*, 1400 – 1403.
[2] G. Eibl, D. Bruemmer, Y. Okada, J. P. Duffy, R. E. Law, H. A. Reber, O. J. Hines, *Biochem. Biophys. Res. Commun.* **2003**, *306*, 887 – 897.
[3] T. Hida, Y. Yatabe, H. Achiwa, H. Muramatsu, K. Kozaki, S. Nakamura, M. Ogwa, T. Mitsudomi, T. Sugiura, T. Takahashi, *Cancer Res.* **1998**, *58*, 3761 – 37634.
[4] C. H. Koehne, R. N. Dubois, *Semin. Oncol.* **2004**, *31*, 12 – 21.
[5] E. G. Roberts, L. Vona-Davis, D. R. Riggs, B. J. Jackson, H. Hohseni, S. J. Dandzari, D. W. McFadden, *W. Va. Med. J.* **2004**, *100*, 96 – 101.
[6] O. N. Tucker, A. J. Dannenberg, E. K. Yang, F. Zhang, L. Teng, J. M. Daly, R. A. Soslow, J. L. Masferrer, B. M. Woerner, A. T. Koki, T. J. Fahey, *Cancer Res.* **1999**, *59*, 987 – 990.
[7] E. S. Borda, A. Tenenbaum, M. E. Sales, L. Rumi, L. Sterin-Borda, *Prostaglandins Leukotrienes Essent. Fatty Acids* **1998**, *58*, 85 – 90.
[8] S. E. Wenzel, *Pharmacotherapy* **1997**, *17*, 3S – 12S.
[9] R. Pai, B. Soreghan, I. L. Sazabo, M. Pavelka, D. Baatar, A. S. Tarnawski, *Nat Med.* **2002**, *8*, 289 – 293.
[10] A. Castonguay, N. Rioux, C. Duperron, G. Jalbert, *Exp. Lung Res.* **1998**, *24*, 605 – 615.
[11] T. Yamaki, K. Endoh, M. Miyahara, I. Nagamine, N. Thi Thu Huoing, H. Sakurai, J. Pokorny, T. Yano, *Cancer Lett.* **2004**, *214*, 115 – 120.
[12] A. Pozzi, X. Yan, I. Macias-Perez, S. Wei, A. N. Hata, R. M. Breyer, J. D. Morrow, J. H. Capdevila, *J. Biol. Chem.* **2004**, *279*, 29797 – 29804.
[13] H. F. Cheng, R. C. Harris, *Hypertension* **2004**, *43*, 525 – 530.
[14] J. W. Kim, Y. Zou, S. Yoon, J. H. Lee, Y. K. Kim, B. P. Yu, H. Y. Chung, *J. Gerontol. Ser. A* **2004**, *59*, B876 – 885.
[15] J. J. Monsuez, *Arch. Mal. Coeur Vaiss.* **2004**, *97*, 632 – 640.
[16] R. E. Harris, J. Beebe-Donk, H. M. Schuller, *Oncol. Rep.* **2002**, *9*, 693 – 695.
[17] H. M. Schuller, L. Zhang, D. L. Weddle, A. Castonguay, K. Walker, M. S. Miller, *J. Cancer Res. Clin. Oncol.* **2002**, *128*, 525 – 532.
[18] H. Krum, D. Liew, J. Aw, S. Haas, *Expert Rev. Cardiovasc. Ther.* **2004**, *2*, 265 – 270.
[19] J. Couzin, *Science* **2004**, *306*, 2170.
[20] H. M. Schuller, *Nat. Rev. Cancer* **2002**, *2*, 455 – 463.
[21] H. M. Schuller, M. Cekanova, *Lung Cancer* **2004**, *49*, 35 – 45.
[22] G. W. Kabalka, A. R. Mereddy, H. M. Schuller, *J. Labelled Compd. Radiopharm.* **2005**, *4*, 295 – 300.
[23] F. R. Wust, A. Hohne, P. Metz, *Org. Biomol. Chem.* **2005**, *3*, 503 – 507.
[24] E. F. de Vries, A. van Waarde, A. R. Buursma, W. Vaalburg, *J. Nucl. Med.* **2003**, *44*, 1700 – 1706.
[25] T. J. McCarthy, A. U. Sheriff, M. J. Graneto, J. J. Talley, M. J. Welch, *J. Nucl. Med.* **2002**, *43*, 117 – 124.
[26] D. J. Yang, J. Bryant, J. Y. Chang, R. Mendez, C. S. Oh, D. F. Yu, M. Ito, A. Azhdarinia, S. Kohamin, K. E. Edmund, E. Lin, D. A. Podoloff, *Anticancer Drugs* **2004**, 15, 255 – 263.
[27] C. Yokota, T. Kaji, Y. Kuge, H. Inoue, N. Tamaki, K. Minematsu, *Neurosci. Lett.* **2004**, *357*, 210 – 222.
[28] F. Cipollone, B. Rocca, C. Patrono, *Arterioscler. Thromb. Vasc. Biol.* **2004**, *24*, 246 – 255.
[29] J. J. Hoozemans, R. Veerhuis, A. J. Rozemuller, T. Arendt, P. Eikelenboom, *Neurobiol. Dis.* **2004**, *11*, 492 – 499.
[30] J. J. Hoozemans, R. Veerhuis, A. J. Rozemuller, P. Eikelenboom, *Curr. Drug Targets* **2003**, *4*, 4461 – 4468.
[31] C. Fenton, G. M. Keating, A. J. Wagstaff, *Drugs* **2004**, *64*, 1231 – 1261.
[32] R. Wigand, M. Wehling, H. B. Brauer, E. Stridde, H. Vergin, M. May, *Dtsch. Med. Wochenschr.* **2004**, *129*, 1188 – 1192.
[33] P. Juni, L. Nartey, S. Reichenbach, R. Sterchi, P. A. Dieppe, M. Egger, *Lancet* **2004**, 364.
[34] T. Saito, I. W. Rodger, H. Shennib, F. Hu, L. Tayara, A. Biaid, *Can. J. Physiol. Pharmacol.* **2003**, *81*, 114 – 119.
[35] Y. Kuge, Y. Kadada, S. Shimonaka, T. Temma, H. Kimura, Y. Kiyono, C. Yokota, K. Minematsu, K. Seti, N. Tamaki, K. Ohkura, H. Sayi, *Nucl. Med. Biol.* **2006**, *33*, 21 – 27.
[36] H. Tjalve, *Arch. Exp. Veterinaermed.* **1989**, *43*, 489 – 504.

Received: August 30, 2005
Published online on April 28, 2006

